Journal of Magnetism and Magnetic Materials 475 (2019) 257–263

Contents lists available at ScienceDirect

Journal of Magnetism and Magnetic Materials

journal homepage: www.elsevier.com/locate/jmmm

Research articles

Characterization of Majorana-Ising phase transition in a helical liquid system

Sudip Kumar Saha[a], Dayasindhu Dey[a], Monalisa Singh Roy[a], Sujit Sarkar[b], Manoranjan Kumar[a,*]

[a] S. N. Bose National Centre for Basic Sciences, Block JD, Sector III, Salt Lake, Kolkata 700106, India
[b] Poornaprajna Institute of Scientific Research, 4 Sadashivanagar, Bangalore 560080, India

ARTICLE INFO

Keywords:
Majorana fermion
DMRG
Helical liquid
Spin chain

ABSTRACT

We map an interacting helical liquid system, coupled to an external magnetic field and s-wave superconductor, to an XYZ spin system, and it undergoes Majorana-Ising transition by tuning of parameters. In the Majorana state lowest excitation gap decays exponentially with system size, and the system has degenerate ground state in the thermodynamic limit. On the contrary, the gap opens in the Ising phase even in the thermodynamic limit. We study various criteria to characterize the transition, such as edge spin correlation with its neighbor $C(r = 1)$, local susceptibility χ_l, superconducting order parameter of edge spin $P(r = 1)$, and longitudinal structure factor $S(k)$. All these criteria lead to the same critical value of parameters for Majorana-Ising phase transition in the thermodynamic limit. We study the entanglement spectrum of the reduced density matrix of the helical liquid system. The system shows finite Schmidt gap and non-degeneracy of the entanglement spectrum in the Ising limit. The Schmidt gap closes in the Majorana state, and all the eigenvalues are either doubly or multiply degenerate.

1. Introduction

The Majorana fermion (MF) was first proposed by E. Majorana as a real solution of Dirac equation [1]. In the past few years, understanding MF in condensed matter physics has become a topic of theoretical and experimental research [2,3]. Recent studies show that it exists as quasiparticle excitation in condensed matter system [4–25]. The fact that the exchange of two MF follows non-abelian statistics in contrast to normal bosons and fermions, is useful for quantum computation which is robust against local perturbation [4,26–28]. Kitaev proposed Majorana modes in 1D toy model with proximity induced superconductor [4]. Inspired by Kitaev's work, many other systems are proposed to exhibit Majorana quasiparticle excitation, such as semiconductor-superconductor nano wire [9–15], Bogoliubov quasiparticle in two-dimensional superconductors [5–8], proximity induced topological superconductor [16–23,29], and the cold atoms trapped in one-dimension [24,25].

The real world applications of these fermionic systems depend on the stability of the MF. A single spin polarized fermion band system with spin orbit coupling and proximity induced superconductor shows Majorana like modes in the presence of weak fermionic interaction. However, it was shown that the interaction weakens the stability of the MF [30]. Potter and Lee [21] showed that the $p + ip$ superconductor possesses localized Majorana particles in a rectangular system with width less than the coherence length of the superconductor. The helical liquid system is another candidate where the Majorana like quasi-particles can exist. The helical liquid system generally originates because of the quantum spin Hall effect in a system with or without Landau levels. In this system, a coupling of the left moving down spin with the right moving up spin at the edge of two dimensional quantum hall systems gives rise to a quantized transport process. In this phase, the spin and the momentum degrees of freedom are coupled together without breaking the time reversal symmetry. Various aspects of helical spin liquid is discussed in [31–35].

The field theoretical calculation by Sela et al. [31] shows that the Majorana bound state in a helical liquid possesses a higher degree of stability. In presence of the interaction, the scattering processes between the two constituent fermion bands in the helical liquid system stabilizes the Majorana bound state by opening a gap [22,30–32]. However, the strong interaction may induce decoherence in the Majorana modes. They also considered a highly anisotropic spin model with transverse and longitudinal fields, and the system shows Majorana to Ising transition (MI) [31,32,35]. One of our coauthors showed using RG calculation that a transition from a phase with Majorana edge modes to the Ising phase exists in the helical liquid system for both presence and absence of interaction [32]. However, a systematic and

* Corresponding author.
E-mail addresses: sudipksaha@bose.res.in (S.K. Saha), manoranjan.kumar@bose.res.in (M. Kumar).

https://doi.org/10.1016/j.jmmm.2018.11.088
Received 6 March 2018; Received in revised form 17 September 2018; Accepted 16 November 2018
Available online 17 November 2018
0304-8853/

accurate calculation of the phase boundary of the MI quantum phase transition is still absent in the literature. The above model can be mapped to a one dimensional (1D) XYZ spin-1/2 model. The XYZ model for a spin-1/2 chain can be realised in presence of anisotropic interactions between two neighbouring spins. The zero energy mode (ZEM) in spin chains and spinless fermionic model is explained very well in Ref. [36].

In this paper, we study the existence of the Majorana like ZEM in the spin-1/2 XYZ model, and also propose different criteria to characterize the MI quantum phase transition. We also analyze the entanglement spectrum (ES) to characterize the topological aspects of the ZEM. To understand the ZEM in spin-1/2 XYZ model and for the sake of completeness, let us review the Majorana zero energy modes in helical liquid system [31].

Sela et al. [31] introduced a helical fermionic system, which can be written in the field theoretical representation as

$$H = H_0 + \delta H + H_{fw} + H_{um}, \tag{1}$$

where H_0 and δH include the kinetic energy, single potential energy, external magnetic field, and proximity induced energy terms. H_{fw} and H_{um} represent the forward scattering and the umklapp scattering terms respectively. The H_0 and δH terms can be written more explicitly as

$$\begin{aligned} H_0 &= \int dx\,[\psi^\dagger_{L\downarrow}(v_F i\partial_x - \mu)\psi_{L\downarrow} + \psi^\dagger_{R\uparrow}(-v_F i\partial_x - \mu)\psi_{R\uparrow}], \\ \delta H &= \int dx\,[B\psi^\dagger_{L\downarrow}\psi_{R\uparrow} + \Delta\psi_{L\downarrow}\psi_{R\uparrow} + h.\,c.], \end{aligned} \tag{2}$$

where $\psi_{L\downarrow}$ and $\psi_{R\uparrow}$ are the field operators for left moving down spin and right moving up spin fermions respectively, v_F and μ are the Fermi-velocity and chemical potential of the helical liquid. The system is coupled to the magnetic field B, and Δ is the proximity induced superconducting gap. When a helical liquid system is interfaced with s-wave supercondector, Cooper pairs can tunnel into the surface state of the system due to proximity effect. This phenomenon in the system can be taken care by pairing energy term with amplitude Δ which depends on the nature of the interface of the helical liquid and the superconductor [16,37].

Both the scattering terms are given as

$$\begin{aligned} H_{fw} &= \int dx\left[g_2\psi^\dagger_{L\downarrow}\psi_{L\downarrow}\psi^\dagger_{R\uparrow}\psi_{R\uparrow} + \tfrac{g_4}{2}\{(\psi^\dagger_{L\downarrow}\psi_{L\downarrow})^2 + (\psi^\dagger_{R\uparrow}\psi_{R\uparrow})^2\}\right], \\ H_{um} &= g_u \int dx\,[\psi^\dagger_{L\downarrow}\partial_x\psi^\dagger_{L\downarrow}\psi_{R\uparrow}\partial_x\psi_{R\uparrow} + h.\,c.]. \end{aligned} \tag{3}$$

The conventional analytical expression for the umklapp scattering term H_{um} for the half filling [31,32,35,38] is written in Eq. (3). This analytical expression gives a regularized theory using the lattice constant a as an ultraviolet cut-off.

This complete Hamiltonian in Eq. (1) is mapped to a spin-1/2 *XYZ* model Hamiltonian [31,32,35]

$$\begin{aligned} H = \tfrac{J}{2}\sum_i (S^+_i S^-_{i+1} + S^-_i S^+_{i+1}) + J^z \sum_i S^z_i S^z_{i+1} \\ + \tfrac{\Delta}{2}\sum_i (S^+_i S^+_{i+1} + S^-_i S^-_{i+1}) - \sum_i [\mu + B(-1)^i] S^z_i. \end{aligned} \tag{4}$$

Here, $S^+ = S_x + iS_y$ and $S^- = S_x - iS_y$ are the spin raising and lowering operators and $J = v_F$, Δ is the proximity induced superconducting gap introduced earlier. In spin model this Δ creates the anisotropy in the x and y direction as we can write, without loss of generality, $J^x = J + \Delta$ and $J^y = J - \Delta$. μ and $B$are longitudinal normal and staggered magnetic field applied externally. Here, all the scattering terms of the helical system in Eq. (3) are mapped to the interaction energy of the spin component in $z$direction as $J^z = \frac{g_2}{4} = \frac{g_4}{2} = g_u$.

The spin Hamiltonian in Eq. (4) can be mapped to helical liquid Hamiltonian in Eq. (1) by mapping the spin operators exactly to the spinless fermionic operator by Jordan-Wigner transformation [39] and then expressing the spinless fermionic operators c_i with left and right moving fermions [39] as $c_i \sim e^{i\frac{\pi}{2}x}\psi_{R\uparrow} + e^{-i\frac{\pi}{2}x}\psi_{L\downarrow}$.

To have a better understanding of the Majorana modes, we map this spin system in Eq. (4) to the spinless fermion model as [40]

$$\begin{aligned} H = \frac{-J}{2}\sum_i (c^\dagger_i c_{i+1} + h.\,c.) + J^z \sum_i \left(c^\dagger_i c_i - \frac{1}{2}\right)\left(c^\dagger_{i+1} c_{i+1} - \frac{1}{2}\right) \\ + \frac{\Delta}{2}\sum_i (c^\dagger_{i+1} c^\dagger_i + h.\,c.) - \sum_i [\mu + B(-1)^i]\left(c^\dagger_i c_i - \frac{1}{2}\right). \end{aligned} \tag{5}$$

For better insight, let us try to understand the results in the limiting cases. This model is well studied in the limit of $B = 0$ and $J^z = 0$, and Eq. (5) reduces to 1D Kitaev model [4,41] which is given by

$$\begin{aligned} H = -\frac{J}{2}\sum_i (c^\dagger_i c_{i+1} + h.\,c.) + \frac{\Delta}{2}\sum_i (c^\dagger_{i+1} c^\dagger_i + h.\,c.) \\ - \mu \sum_i \left(c^\dagger_i c_i - \frac{1}{2}\right). \end{aligned} \tag{6}$$

The spinless fermionic operators c_j can be expressed in terms of Majorana operators a_j as

$$c_j = \frac{1}{2}(a_{2j-1} + ia_{2j}) \tag{7}$$

$$c^\dagger_j = \frac{1}{2}(a_{2j-1} - ia_{2j}) \tag{8}$$

Here, $a^\dagger_j$ and a_j are the creation and annihilation operators of j^{th} Majorana fermion. Thus the Eq. (6) can be transformed exactly as

$$H = \frac{i}{2}\sum_j [-\mu a_{2j-1}a_{2j} + \frac{1}{2}(J + \Delta)a_{2j}a_{2j+1} + \frac{1}{2}(-J + \Delta)a_{2j-1}a_{2j+2}]. \tag{9}$$

There are two conditions: first, when $J = \Delta = 0$ and $\mu < 0$, system shows trivial phase and two Majorana operators at each site are paired together to form a ground state with occupation number 0. Secondly, for $J = \Delta > 0$ and $\mu = 0$, the Majorana operators from two neighboring sites are coupled together leaving two unpaired Majorana operators at the two ends, and these two Majorana modes are not coupled to the rest of the chain [4,19]. The fermionic edge state formed with these two end operators has occupation 0 or 1 with degenerate ground state, i.e., generating zero energy excitation modes. However, the bulk properties of these systems can be gapped.

In most of the papers [22,42–45], the ZEM are characterized by exponential decay of the lowest excitation gap with system size, and a large expectation value of the creation operator of the fermion $\langle\psi_1|c^\dagger|\psi_2\rangle$ near the edges of the system, where ψ_1 and ψ_2 are the wave functions of two lowest energy states. However, in the spin language there is no trivial relation between the Majorana mode and spin raising operators. Therefore, in this paper our main focus is to find the accurate phase boundary of the MI transition, and for this purpose we focus on the lowest excitation gap Γ, derivative of longitudinal spin-spin correlations $C(1)$ between edge spin and its nearest neighbor spin, and spin density ρ_e of edge sites. In principle, the ZEM do not couple with the bulk states [4,19]; therefore, this correlation of the edge spin should decay exponentially. We notice that a local magnetic susceptibility χ_i shows a discontinuity near the phase transition. Fifth quantity is $P(r)$ of edge spin, and it is similar to the spin quadrupolar/spin-nematic order parameter [46–48] or superconducting order parameter of model in Eq. (5). The structure factor $S(q)$ gives us information about the phase boundary and the bulk state. Based on the above quantities the MI transition boundary is calculated in this paper. The bulk properties of the Majorana state of the helical liquid is rarely discussed in the literature, however we will try to discuss those properties in this paper. In later part of this paper, the ES of both states are also discussed to understand the topological aspects of Majorana modes.

The Hamiltonian mentioned in Eq. (4) is treated with exact diagonalization (ED) method and Density matrix renormalization group (DMRG) method [49,50]. We have considered open boundary condition of the system to understand the edge modes. The systems with up to

$N = 24$ spins are treated with ED. For higher system sizes, we have used DMRG method. The DMRG is a state of the art numerical technique to solve the $1D$ interacting system, and is based on the systematic truncation of irrelevant degrees of freedom in the Hilbert space [49,50]. This numerical method is best suited to calculate a few low lying excited states of strongly interacting quantum systems accurately. To solve the interacting Hamiltonian for ladder and chain with periodic boundary condition, the DMRG method is further improved by modifying conventional DMRG method [51] for zigzag chains [52], quasi one dimension [53] and higher dimensions [54]. The left and right block symmetry of DMRG algorithm for a XYZ-model of a spin-1/2 chain in a staggered magnetic field (in Eq. (4)) is broken. Therefore, we use conventional unsymmetrized DMRG algorithm [49,50] with open boundary condition. In this model, the total S^z is not conserved as S^z does not commute with the Hamiltonian in Eq. (4). As a result, the superblock dimension is large. We keep $m \sim 500$ eigenvectors corresponding to the highest eigenvalues of the density matrix to maintain the desired accuracy of the results. The truncation error of density matrix eigenvalues is less than 10^{-12}. The energy convergence is better than 0.001% after five finite DMRG sweeps. We go up to $N = 200$ sites for the extrapolation of the transition points.

This paper is divided into three sections. In Section 2, we discuss our numerical results, and this is divided into eight subsections. Results are discussed and compared with the existing literature in Section 3.

2. Numerical results

In this section, various criteria for the MI transition are discussed. We construct a phase diagram in B, Δ and μ parameter space for given $J^z = 0$ and 0.5. Thereafter, various criteria of the MI such as lowest excitation energy Γ, edge spin correlation with its nearest neighbor $C(r = 1)$, local susceptibility at the site nearest neighbor to the edge χ_2, superconducting or spin-nematic order parameter of edge spin $P(r = 1)$, and structure factor $S(k)$ are studied. We show that all these quantities show extrema at a transition parameter B_m in $\Delta - B$ parameter space. However, all these extrema B_m are extrapolated to the same point in the thermodynamic limit, and this extrapolation is done in the Section 2.8. The ES is analyzed in Section 2.7 to show the distinction between topological and the Ising phase.

2.1. Phase diagram

A phase diagram of the model Hamiltonian in Eq. (4), is shown as a color gradient plot in Fig. 1, where the color gradient represents the critical value of Δ, i.e., Δ_c, and X- and Y-axis are the μ and the B of the MI transition points for a system size $N = 100$ for . In the Majorana phase, the lowest excitation gap decays exponentially with system size. The phase diagram shows that a finite Δ_c is required to generate the Majorana modes in a finite system. The μ favors the longitudinal degrees of freedom and tries to induce the ferromagnetic order, although B tries to align the nearest spins in opposite directions to induce the Antiferromagnetic Néel phase. In fact the B and the μ both favor the Ising order, whereas the Δ breaks the parity symmetry and induces the degeneracy in the system. It also induces the formation of Cooper-pairs or magnon-pairs like excitations at the two neighboring sites for the model Hamiltonian given by Eq. (5) or Eq. (4) respectively. As shown in Fig. 1, the Δ_c increases with increasing $B$for a fixed value of μ, and it increases with increasing μ for a given B. The trends are similar for both $J^z = 0$ and 0.5.

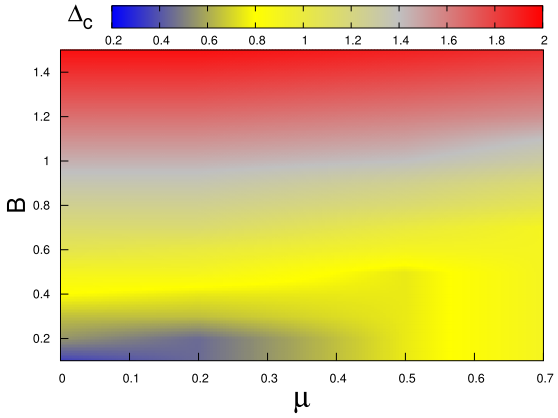

Fig. 1. MI phase boundary for a helical liquid mentioned in Eq. (4) in the parameter space of μ and $B$for $J^z = 0.5$. The color gradient represents the critical values of Δ on the phase boundary, i.e., Δ_c.

2.2. Excitation gap Γ

To characterize the Majorana modes in one dimension for the helical system, the lowest excitation gap Γ is defined as

$$\Gamma = E_1(\Delta, \mu, B) - E_0(\Delta, \mu, B), \tag{10}$$

where E_0 and E_1 are ground state and lowest excited state of the Hamiltonian in Eq. (4). The $\Gamma - N$ is plotted in log-linear scale in Fig. 2. The $\Gamma - N$ plot for $\mu = 0.0$, $\Delta = 0.5$, $J^z = 0.5$, and for five values of B. For $B = 0.05$, 0.1 and 0.15, Γ shows the exponential decay (Majorana regime), whereas Γ goes linearly with $1/N$ for $B = 0.2$ and 0.25 (Ising phase) as shown in the Fig. 2. The phase boundary of MI transition is evaluated based on change in $\Gamma - N$ relation from exponential to the power law. We also notice that the contribution to the excitation gap Γ is uniformly distributed in the Ising phase, whereas, in the Majorana state, the major contribution comes from the edge as shown in Fig. 5 of [35].

2.3. Correlation function $C(r = 1)$ from the edge

The longitudinal spin-spin correlation fluctuation $C(r)$ at a distance r from reference point i is defined as

$$C(r) = \langle S_i^z S_{i+r}^z \rangle - \langle S_i^z \rangle \langle S_{i+r}^z \rangle, \tag{11}$$

where $\langle S_i^z \rangle$ and $\langle S_{i+r}^z \rangle$ are spin densities at the reference site i and other site $i + r$. In Fig. 3, the edge spin site $i = 1$ is considered as the reference spin. The distance dependence of $C(r)$ for $\mu = 0$, $J^z = 0$ and $\Delta = 0.5$ is shown in inset of Fig. 3. It decreases exponentially for $r \geqslant 2$, and effectively, only last two sites are correlated. Therefore, $C(r = 1)$ between

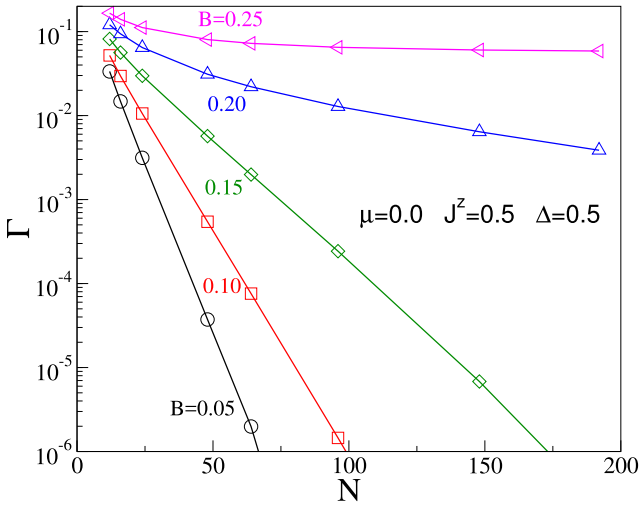

Fig. 2. Lowest excitation gap Γ (in Eq. (10)) vs. the system size N for $\mu = 0$, $J^z = 0.5$ and $\Delta = 0.5$ with different values of B chosen around the $B_c = 0.15$ (see Fig. 1).

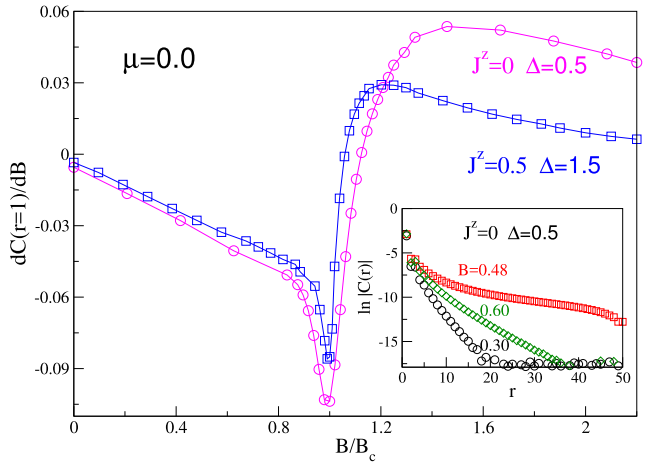

Fig. 3. The derivative of longitudinal spin-spin correlation between the spins corresponding to the edge bond $dC(r=1)/dB$ with the staggered magnetic field B both for ($\Delta = 0.5$, $\mu = J^z = 0$) and ($\Delta = 1.5$, $J^z = 0.5$, $\mu = 0$). The inset shows the distance dependence of $\ln|C(r)|$ for $B = 0.3$, 0.48 and 0.6 and for $\Delta = 0.5$, $\mu = J^z = 0$.

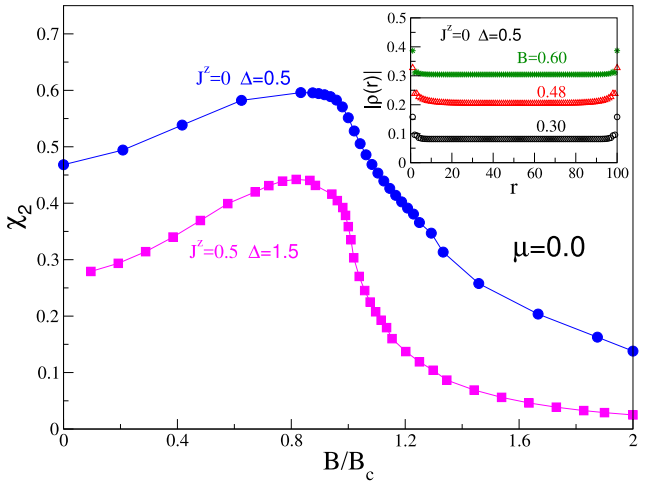

Fig. 4. Local staggered magnetic susceptibility (in Eq. (10)) of the second site nearest neighbor to the edge χ_2 vs. B/B_c both for ($\Delta = 0.5$, $\mu = J^z = 0$) and ($\Delta = 1.5$, $J^z = 0.5$, $\mu = 0$). In the inset, the spin density $\rho(r)$ for the whole system for $B = 0.3$, 0.48 and 0.6 with $\Delta = 0.5$, $\mu = J^z = 0$ is shown.

nearest neighbors is important. $C(r=1)$ first increases with B in the Majorana state and decreases afterwards in the Ising phase. The $dC(r=1)/dB$ is plotted as a function of B/B_c in the main Fig. 3 for ($J^z = 0$, $\Delta = 0.5$), and ($J^z = 0.5$, $\Delta = 1.5$) and $\mu = 0$. This minimum for the given value of parameters is also consistent with the MI transition point calculated from energy degeneracy.

2.4. Local magnetic susceptibility χ_i

The Majorana modes are confined to the edge of the system, therefore we focus on the spin density of edge sites $i = 1$ and 2 for $\Delta = 0.5$, $\mu = 0$ and $J^z = 0$. The spin density and the local staggered magnetic susceptibility is defined as

$$\rho_i = 2\langle S_i^z \rangle, \tag{12}$$

$$\chi_i = \left| \frac{d\rho_i}{dB} \right|, \tag{13}$$

where, $\langle S_i^z \rangle$ are the longitudinal spin density at site i. The magnitude of spin density ρ_i for site $i = 1$, 2 increases at both the sites with B, it is positive at site 1 and negative at site 2. The magnitude of ρ_i at site 2 is lower than that is at site 1. However, both of them saturate with high staggered field, but ρ_1 continuously increases and there is no maxima for this function. The χ_2 as a function of B/B_c are plotted in the main Fig. 4 for ($J^z = 0$, $\Delta = 0.5$) and ($J^z = 0.5$, $\Delta = 1.5$) and both for $\mu = 0$. These two functions show a maxima near the transition. The ρ_i for the whole system for $J^z = 0$, $\Delta = 0.5$ and $\mu = 0$ is shown in the inset of Fig. 4. We notice that the variation of ρ_i is confined to the edge and the first few neighboring sites, and has constant value throughout the rest of system. The ρ_i for $J^z = 0.5$, $\Delta = 1.5$ and $\mu = 0$ behaves in a similar manner.

2.5. Quadrupolar order parameter $P(r=1)$

The third term of the Hamiltonian in Eq. (4) induces the spin quadrupolar/spin-nematic order in the system. In this phase $\langle S^+ \rangle$ vanishes, whereas $\langle S^+ S^+ \rangle$ has non-zero value, and two magnon pair formation is favored similar to superconductor system where two electrons form singlet Cooper pair. The spin distance dependent quadrupolar order parameter is defined as

$$P(r) = \langle S_i^x S_{i+r}^x \rangle - \langle S_i^y S_{i+r}^y \rangle,$$
$$= \langle S_i^+ S_{i+r}^+ + S_i^- S_{i+r}^- \rangle. \tag{14}$$

$P(r)$ is the difference in the X and Y component of correlation $\langle \vec{S_i} \cdot \vec{S_{i+r}} \rangle$. For $r = 1$, this quantity is very similar to the spin quadrupolar or superconducting order parameter of the spinless fermion model. The $P(r=1)$ is calculated as a function of B for ($\Delta = 0.5$, $J^z = 0$) and ($\Delta = 1.5$, $J^z = 0.5$) and both for $\mu = 0$, and we notice that when Δ dominates over B, the system goes from non-degenerate Ising phase to doubly degenerate states which favors Majorana edge state and the bulk phase goes to spin quadrupolar phase as $P(r) \neq 0$. The $P(r=1)$ first increases with B, and then it saturates with higher B. The derivative of $P(r=1)$ with B for ($\Delta = 0.5$, $J^z = 0$, $\mu = 0$) and ($\Delta = 1.5$, $J^z = 0.5$, $\mu = 0$) shows maxima at $B = 0.48$ and $B = 1.04$ respectively as shown in the main Fig. 5. The distance dependence of $P(r)$ as a function r are shown for both the regime of the Majorana modes and the Ising states in inset of Fig. 5. The reference site i is the edge site of the chain. In the Majorana state P(r) shows long range behavior, however, it decays exponentially in case of Ising phase.

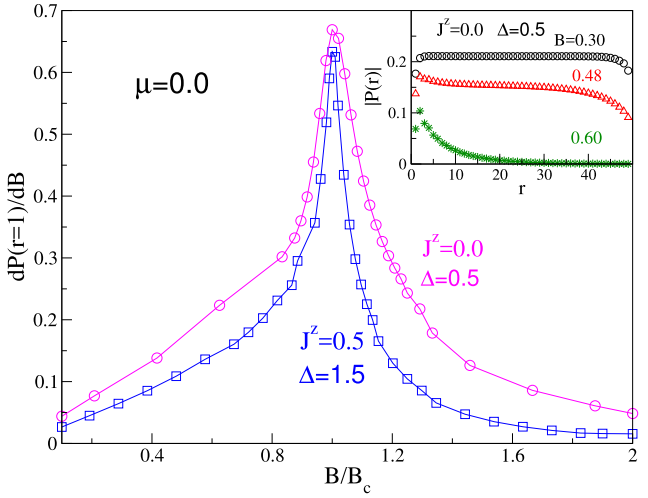

Fig. 5. $\frac{dP(r=1)}{dB}$ as a function of $\frac{B}{B_c}$ is shown in the main figure for ($\Delta = 0.5$, $\mu = J^z = 0$) and ($\Delta = 1.5$, $J^z = 0.5$, $\mu = 0$). $P(r)$ (in Eq. (14)) is plotted for the whole system in the inset for $B = 0.3$, 0.48 and 0.6 with $\Delta = 0.5$, $\mu = J^z = 0$.

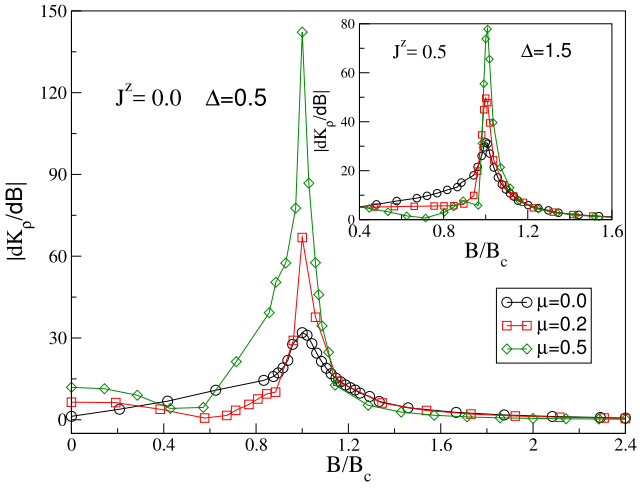

Fig. 6. Derivative of K_ρ (in Eq. (16)) with the staggered magnetic field B, as a function of $\frac{B}{B_c}$ is shown in the main figure for $\Delta = 0.5$, $J^z = 0$, and the inset shows the same for $\Delta = 1.5$, $J^z = 0.5$ for $\mu = 0$, 0.2 and 0.5.

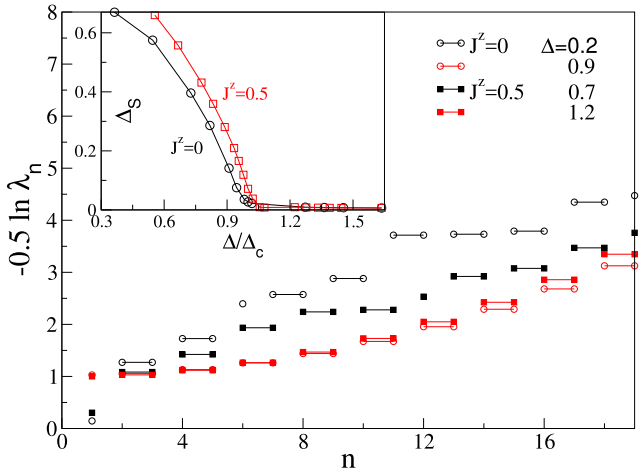

Fig. 7. The entanglement spectrum λ_n is plotted for $\mu = 0$ and $B = 0.5$ in both the Ising and Majorana regime for $J^z = 0$ and $J^z = 0.5$ in the main figure. In the inset, the Schmidt gap Δ_S is shown as a function of $\frac{\Delta}{\Delta_c}$ for $B = 0.5$, $\mu = 0$ both for $J^z = 0$ and $J^z = 0.5$.

2.6. Longitudinal structure factor $S(k)$

The longitudinal structure factor $S(k)$ is the Fourier transformation of $C(r)$ given in Eq. (11), and can be defined as

$$S(k) = \sum_r \left(\langle S_i^z S_{i+r}^z\rangle - \langle S_i^z\rangle\langle S_{i+r}^z\rangle\right)e^{ikr}. \tag{15}$$

Now let us define a quantity K_ρ in small k limit defined as

$$K_\rho = \frac{S(k)}{k/\pi}; k \to 0, \tag{16}$$

where $k = \frac{2\pi m}{N}; m = 0, \pm1, \pm2, ..., \pm\frac{N}{2}$. K_ρ is proportional to the Luttinger Liquid parameter [55–57]. We take the value of the function $\frac{\pi S(k)}{k}$ at $k = \frac{2\pi}{N}(m = 1)$. We calculate K_ρ for the $(\Delta = 0.5, J^z = 0)$ and $(\Delta = 1.5, J^z = 0.5)$ as a function of μ and B. The derivative of K_ρ as a function of B shows maxima at $B = 0.48$, 0.52, and 0.7 for $\mu = 0$, 0.2 and 0.5 at $J^z = 0$ and $\Delta = 0.5$. The derivative of K_ρ with B/B_c for $(\Delta = 0.5, J^z = 0)$ and $(\Delta = 1.5, J^z = 0.5)$ is shown for three different values of μ in the main and in the inset of Fig. 6. The maxima of $\frac{dK_\rho}{dB}$ indicates the boundary between the Majorana and the Ising state. The extrapolated value of the transition point is very close to the transition point calculated from other criteria. It also shows that the critical value of B for the transition calculated from $\frac{dK_\rho}{dB}$ at a fixed Δ increases with increasing μ.

2.7. Entanglement spectrum in Ising and Majorana state

We study the entanglement spectrum (ES) of the reduced density matrix of the helical liquid system to investigate the topological aspect of the Majorana modes [58–60]. For this purpose we consider the bipartition of the full system into two halves, the system (A) and the environment (B). The reduced density matrix for part A is obtained by tracing out the degrees of freedom in part B. For the wave function $|\psi\rangle$ the reduced density matrix for part A is given by $\rho_A = \mathrm{Tr}_B|\psi\rangle\langle\psi|$. ρ_A contains the information of the entanglement between part A and B. The eigen values (λ_n, where $n = 0, 1, 2, ...$) of the reduced density matrix is known as the ES. In Majorana phase, all the states in the ES are either doubly or multiply degenerate [58,59]. The difference between the largest and the second largest eigenvalues, i.e., λ_0 and λ_1 of the ES is called the Schmidt gap $\Delta_S = \lambda_0 - \lambda_1$. Topological phases are also characterized by $\Delta_S = 0$, whereas it is finite in the trivial phase [59].

The ES of the reduced density matrix is analyzed for a chain of $N = 96$ spins with PBC in the deep Ising state ($J^z = 0$, $\Delta = 0.2$ and $J^z = 0.5$, $\Delta = 0.7$), and in the deep Majorana state ($J^z = 0$, $\Delta = 0.9$ and $J^z = 0.5$, $\Delta = 1.2$) for $B = 0.5$ and $\mu = 0$ in the main of Fig. 7. We plot the Schmidt gap (Δ_S) as a function of $\frac{\Delta}{\Delta_c}$ for $J^z = 0$ and shown in the inset of Fig. 7 for the same values of μ and B. We notice that λ_0 is non-degenerate in the Ising state and Schmidt gap is finite in this regime ($\frac{\Delta}{\Delta_c} < 1$) but goes to zero in the Majorana regime ($\frac{\Delta}{\Delta_c} > 1$) as shown in the inset of Fig. 7. In the Ising phase many of λ_n are non-degenerate for ($J^z = 0, \mu = 0, B = 0.5, \Delta = 0.2$) and ($J^z = 0.5, \mu = 0.0, B = 0.5, \Delta = 0.7$). In this phase the ES is of mixed type. The spectrum is shown as open and filled symbols in the main Fig. 7 for $J^z = 0$ and 0.5 respectively. In the Majorana phase the λ_0 is triply degenerate, and for other higher n, these are either doubly or multiply degenerate as shown in the main Fig. 7 for ($J^z = 0, \mu = 0, B = 0.5, \Delta = 0.9$) and ($J^z = 0.5, \mu = 0, B$ =0.5, $\Delta = 1.2$). The phase boundary of the system can be characterized at the point where Schmidt gap goes to zero and the whole spectrum becomes doubly or multiply degenerate. In the Majorana phase first few largest λ_n are independent of parameters.

2.8. MI phase boundary

In the last seven subsections, different criteria give us different MI phase boundary in a finite system size and the phase boundary B_c, calculated from different criteria have different finite size dependence. For $\mu = 0.2$, the finite size scaling of the B_c for four different criteria, i.e., ground state degeneracy (GSD), K_ρ, $P(r = 1)$ and $C(r = 1)$ are shown in the inset (a) of Fig. 8. The GSD and $C(r = 1)$ have same finite size effect. We notice that the extrapolations from all the criteria lead to the same $B_c = 0.52$ in the thermodynamic limit. The effect of μ on the MI transition point B_c is shown in the thermodynamic limit for ($J^z = 0, \Delta = 0.5$) and ($J^z = 0.5, \Delta = 1.5$) in the main Fig. 8. We have also shown the effect of J^z on the MI transition in the thermodynamic limit in the inset (b) both for ($\mu = 0, \Delta = 1.0$) and ($\mu = 0.2, \Delta = 1.5$).

3. Discussion

We have studied the helical liquid system and mapped this model into a *XYZ*spin-1/2 chain model. The Majorana-Ising transition is characterized by calculating the lowest excitation gap of the model Hamiltonian in Eq. (4) on a chain geometry. In the Majorana state, the system has finite gap for a finite system which decays exponentially with the system size N. The closing of the gap in the thermodynamic

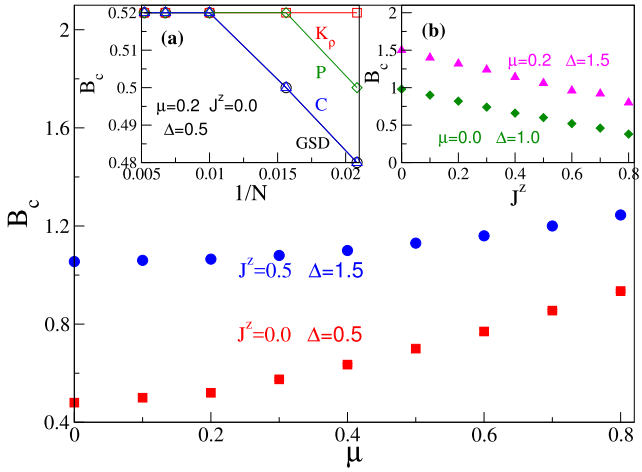

Fig. 8. The effect of μ on the MI transition in the thermodynamic limit both for $J^z = 0$, $\Delta = 0.5$ and $J^z = 0.5$, $\Delta = 1.5$ are shown in the main figure. The finite size scaling of B_c from different criteria, i.e., GSD, $C(r)$, $P(r)$ and K_ρ, is shown for $J^z = 0$, $\Delta = 0.5$ and $\mu = 0.2$ in the inset (a). The inset (b) shows the effect of J^z on the MI transition boundary in the thermodynamic limit both for $\mu = 0$, $\Delta = 1.0$ and $\mu = 0.2$, $\Delta = 1.5$.

limit is consistent with the study by Sela et al. [31]. Our aim of this paper is to explore various criteria to characterize Majorana mode other than closing of the lowest excitation gap, and the accurate determination of the MI transition boundary in an anisotropic XYZ spin-1/2 model in Eq. (4). We have calculated various quantities, e.g., ρ_i, $C(r)$, $P(r)$, K_ρ, Δ_S. We have shown that the phase boundary calculated from the various criteria are the same for given value of Δ and μ in the thermodynamic limit. We have shown that in strong repulsive interaction limit $J^z > 0$, Majorana mode occurs at higher value of Δ than the non-interacting case ($J^z = 0$), which is consistent with the study of Gangadharaiah et al. [30], where they have shown that the repulsive interaction weakens the Majorana modes. The J^z term of Eq. (4) is similar to the repulsive interaction term of the spinless fermion model in Eq. (5). In the mean field limit, J^z term reduces to effective μ. The $P(r)$ is long range in the Majorana state, whereas it decays exponentially in the Ising phase as shown in the inset of Fig. 5. In the Majorana state, the bulk of system shows quadrupolar/or spin nematic phase like behavior. The local magnetic susceptibility at the site nearest neighbor to the edge site, i.e., χ_2 shows maxima near the phase boundary.

We have also studied the ES of this model, and it is shown that the Ising phase has finite Schmidt gap Δ_S, and non-degenerate eigenvalues are present in the spectrum of the reduced density matrix of the system, whereas the topological aspect of Majorana state is characterized by the doubly degenerate eigenvalues and zero Schmidt gap [58,59]. We have also shown that ES of the reduced density matrix of the ground state shows double and multiple degeneracy in the Majorana state. We have also noticed threefold degeneracy in the largest eigenvalues in this state in the thermodynamic limit. Degeneracy of all the eigenvalues is very similar to the study by Pollmann et al. [58] to distinguish the topological and trivial phase of $S = 1$ system. The first few eigenvalues of ES in the Majorana state is almost independent of parameters as shown in Fig. 7.

In conclusion, we have studied the helical liquid phase in one dimensional system. This system shows the Majorana-Ising transition, and the phase boundary is calculated using various criteria. The topological aspect of the Majorana modes is studied for helical model, and the closing of the Schmidt gap and degeneracy of full spectrum of reduced density matrix can also be used to characterize the phase boundary of Majorana-Ising transition. This model is one of the most interesting and a general model for spin-1/2 systems. Our study shows that an anisotropic spin-1/2 chain can be a good candidate to observe the Majorana modes and MI transition. The local experimental probe like neutron magnetic resonance can be used to measure the local spin density at the edge of the sample.

Acknowledgements

MK thanks Z. G. Soos and Sumanta Tewari for their valuable comments. MK thanks DST for a Ramanujan Fellowship SR/S2/RJN-69/2012 and funding computation facility through SNB/MK/14-15/137. SS thanks the DST (SERB, SR/S2/LOP-07/2012) fund and SNBNCBC for supporting the visit and also the academic activities of ICTS/TIFR. SKS thanks DST-INSPIRE for financial support.

References

[1] E. Majorana, Teoria simmetrica dell'elettrone e del positrone, Nuovo Cimento 14 (1937) 171, https://doi.org/10.1007/BF02961314.
[2] F. Wilczek, Majorana returns, Nat. Phys. 5 (2009) 614, https://doi.org/10.1038/nphys1380.
[3] B.A. Bernevig, T.L. Hughes, Topological Insulators and Topological Superconductors, Princeton University Press, Princeton, 2013.
[4] A.Y. Kitaev, Unpaired majorana fermions in quantum wires, Physics-Uspekhi 44 (2001) 131.
[5] D.A. Ivanov, Non-abelian statistics of half-quantum vortices in p-wave superconductors, Phys. Rev. Lett. 86 (2001) 268–271, https://doi.org/10.1103/PhysRevLett. 86.268.
[6] Y.E. Kraus, A. Auerbach, H.A. Fertig, S.H. Simon, Majorana fermions of a two-dimensional p_x + ip_y superconductor, Phys. Rev. B 79 (2009) 134515, https://doi.org/10.1103/PhysRevB.79.134515.
[7] M. Wimmer, A.R. Akhmerov, M.V. Medvedyeva, J. Tworzydło, C.W.J. Beenakker, Majorana bound states without vortices in topological superconductors with electrostatic defects, Phys. Rev. Lett. 105 (2010) 046803, https://doi.org/10.1103/PhysRevLett. 105.046803.
[8] M. Sato, S. Fujimoto, Majorana fermions and topology in superconductors, J. Phys. Soc. Jpn. 85 (2016) 72001, https://doi.org/10.7566/JPSJ.85.072001.
[9] T.D. Stanescu, S. Tewari, Majorana fermions in semiconductor nanowires: fundamentals, modeling, and experiment, J. Phys.: Condens. Matter 25 (2013) 233201, https://doi.org/10.1088/0953-8984/25/23/233201.
[10] V. Mourik, K. Zuo, S.M. Frolov, S.R. Plissard, E.P.A.M. Bakkers, L.P. Kouwenhoven, Signatures of majorana fermions in hybrid superconductor-semiconductor nanowire devices, Science 336 (6084) (2012) 1003–1007, https://doi.org/10.1126/science.1222360.
[11] M.T. Deng, C.L. Yu, G.Y. Huang, M. Larsson, P. Caroff, H.Q. Xu, Anomalous zero-bias conductance peak in a nb insb nanowire nb hybrid device, Nano Lett. 12 (2012) 6414–6419, https://doi.org/10.1021/nl303758w.
[12] L.P. Rokhinson, X. Liu, J.K. Furdyna, The fractional a.c. josephson effect in a semiconductor-superconductor nanowire as a signature of majorana particles, Nat. Phys. 8 (2012) 795, https://doi.org/10.1038/nphys2429.
[13] A. Das, Y. Ronen, Y. Most, Y. Oreg, M. Heiblum, H. Shtrikman, Zero-bias peaks and splitting in an al inas nanowire topological superconductor as a signature of majorana fermions, Nat. Phys. 8 (2012) 887, https://doi.org/10.1038/nphys2479.
[14] A.D.K. Finck, D.J. Van Harlingen, P.K. Mohseni, K. Jung, X. Li, Anomalous modulation of a zero-bias peak in a hybrid nanowire-superconductor device, Phys. Rev. Lett. 110 (2013) 126406, https://doi.org/10.1103/PhysRevLett. 110.126406.
[15] R. Jafari, A. Langari, A. Akbari, K.-S. Kim, Real space renormalization of majorana fermions in quantum nano-wire superconductors, J. Phys. Soc. Jpn. 86 (2017) 024008, https://doi.org/10.7566/JPSJ.86.024008.
[16] L. Fu, C.L. Kane, Superconducting proximity effect and majorana fermions at the surface of a topological insulator, Phys. Rev. Lett. 100 (2008) 096407, https://doi.org/10.1103/PhysRevLett. 100.096407.
[17] L. Fu, C.L. Kane, Josephson current and noise at a superconductor/quantum-spin-hall-insulator/superconductor junction, Phys. Rev. B 79 (2009) 161408, https://doi.org/10.1103/PhysRevB.79.161408.
[18] J. Alicea, Majorana fermions in a tunable semiconductor device, Phys. Rev. B 81 (2010) 125318, https://doi.org/10.1103/PhysRevB.81.125318.
[19] J. Alicea, New directions in the pursuit of majorana fermions in solid state systems, Rep. Prog. Phys. 75 (7) (2012) 076501 .
[20] J.D. Sau, R.M. Lutchyn, S. Tewari, S. Das Sarma, Generic new platform for topological quantum computation using semiconductor heterostructures, Phys. Rev. Lett. 104 (2010) 040502, https://doi.org/10.1103/PhysRevLett.104.040502.
[21] A.C. Potter, P.A. Lee, Multichannel generalization of kitaev's majorana end states and a practical route to realize them in thin films, Phys. Rev. Lett. 105 (2010) 227003, https://doi.org/10.1103/PhysRevLett. 105.227003.
[22] E.M. Stoudenmire, J. Alicea, O.A. Starykh, M.P.A. Fisher, Interaction effects in topological superconducting wires supporting majorana fermions, Phys. Rev. B 84 (2011) 014503, https://doi.org/10.1103/PhysRevB.84.014503.
[23] T. Fukui, T. Fujiwara, Topological stability of majorana zero modes in superconductor topological insulator systems, J. Phys. Soc. Jpn. 79 (3) (2010) 033701, https://doi.org/10.1143/JPSJ.79.033701.
[24] C. Zhang, S. Tewari, R.M. Lutchyn, S. Das Sarma, $p_x + ip_y$, Phys. Rev. Lett. 101 (2008) 160401, https://doi.org/10.1103/PhysRevLett. 101.160401.

[25] L. Jiang, T. Kitagawa, J. Alicea, A.R. Akhmerov, D. Pekker, G. Refael, J.I. Cirac, E. Demler, M.D. Lukin, P. Zoller, Majorana fermions in equilibrium and in driven cold-atom quantum wires, Phys. Rev. Lett. 106 (2011) 220402, https://doi.org/10.1103/PhysRevLett. 106.220402.
[26] C. Nayak, S.H. Simon, A. Stern, M. Freedman, S. Das Sarma, Non-abelian anyons and topological quantum computation, Rev. Mod. Phys. 80 (2008) 1083–1159, https://doi.org/10.1103/RevModPhys.80.1083.
[27] J.D. Sau, S. Tewari, S. Das Sarma, Universal quantum computation in a semiconductor quantum wire network, Phys. Rev. A 82 (2010) 052322, https://doi.org/10.1103/PhysRevA.82.052322.
[28] J. Alicea, Y. Oreg, G. Refael, F. von Oppen, M.P.A. Fisher, Non-abelian statistics and topological quantum information processing in 1d wire networks, Nat. Phys. 7 (2011) 412, https://doi.org/10.1038/nphys1915.
[29] S. Sarkar, Topological quantum phase transition and local topological order in a strongly interacting light-matter system, Sci. Rep. 7 (2017) 1840, https://doi.org/10.1038/s41598-017-01726-z.
[30] S. Gangadharaiah, B. Braunecker, P. Simon, D. Loss, Majorana edge states in interacting one-dimensional systems, Phys. Rev. Lett. 107 (2011) 036801, https://doi.org/10.1103/PhysRevLett. 107.036801.
[31] E. Sela, A. Altland, A. Rosch, Majorana fermions in strongly interacting helical liquids, Phys. Rev. B 84 (2011) 085114, https://doi.org/10.1103/PhysRevB.84.085114.
[32] S. Sarkar, Physics of majorana modes in interacting helical liquid, Sci. Rep. 6 (2016) 30569, https://doi.org/10.1038/srep30569.
[33] X.-L. Qi, S.-C. Zhang, The quantum spin hall effect and topological insulators, Phys. Today 63 (2010) 33, https://doi.org/10.1063/1.3293411.
[34] X.-L. Qi, S.-C. Zhang, Topological insulators and superconductors, Rev. Mod. Phys. 83 (2011) 1057–1110, https://doi.org/10.1103/RevModPhys. 83.1057.
[35] D. Dey, S.K. Saha, P.S. Deo, M. Kumar, S. Sarkar, A study of topological quantum phase transition and majorana localization length for the interacting helical liquid system, J. Phys. Soc. Jpn. 86 (2017) 074002, https://doi.org/10.7566/JPSJ.86.074002.
[36] P. Fendley, Parafermionic edge zero modes in z n-invariant spin chains, J. Stat. Mech. 2012 (11) (2012) P11020 URL: http://stacks.iop.org/1742-5468/2012/i=11/a=P11020.
[37] A. Volkov, P. Magne, B. van Wees, T. Klapwijk, Proximity and josephson effects in superconductor-two-dimensional electron gas planar junctions, Physica 242C (1995) 261–266, https://doi.org/10.1016/0921-4534(94)02429-4.
[38] C. Wu, B.A. Bernevig, S.-C. Zhang, Helical liquid and the edge of quantum spin hall systems, Phys. Rev. Lett. 96 (2006) 106401, https://doi.org/10.1103/PhysRevLett.96.106401.
[39] E. Fradkin, Field Theories of Condensed Matter Physics, Cambridge University Press, 2013.
[40] H. Katsura, D. Schuricht, M. Takahashi, Exact ground states and topological order in interacting kitaev/majorana chains, Phys. Rev. B 92 (2015) 115137, https://doi.org/10.1103/PhysRevB.92.115137.
[41] K. Kawabata, R. Kobayashi, N. Wu, H. Katsura, Exact zero modes in twisted kitaev chains, Phys. Rev. B 95 (2017) 195140, https://doi.org/10.1103/PhysRevB.95.195140.
[42] N.M. Gergs, L. Fritz, D. Schuricht, Topological order in the kitaev/majorana chain in the presence of disorder and interactions, Phys. Rev. B 93 (2016) 075129, https://doi.org/10.1103/PhysRevB.93.075129.
[43] A. Rahmani, X. Zhu, M. Franz, I. Affleck, Phase diagram of the interacting majorana chain model, Phys. Rev. B 92 (2015) 235123, https://doi.org/10.1103/PhysRevB.92.235123.
[44] W. Zhu, S.S. Gong, F.D.M. Haldane, D.N. Sheng, Topological characterization of the non-abelian moore-read state using density-matrix renormalization group, Phys. Rev. B 92 (2015) 165106, https://doi.org/10.1103/PhysRevB.92.165106.
[45] S. Ejima, H. Fehske, Comparative density-matrix renormalization group study of symmetry-protected topological phases in spin-1 chain and bose-hubbard models, Phys. Rev. B 91 (2015) 045121, https://doi.org/10.1103/PhysRevB.91.045121.
[46] A. Parvej, M. Kumar, Multipolar phase in frustrated spin-1/2 and spin-1 chains, Phys. Rev. B 96 (2017) 054413, https://doi.org/10.1103/PhysRevB.96.054413.
[47] C. Luo, T. Datta, D.-X. Yao, Spin and quadrupolar orders in the spin-1 bilinear-biquadratic model for iron-based superconductors, Phys. Rev. B 93 (2016) 235148, https://doi.org/10.1103/PhysRevB.93.235148.
[48] S.-S. Gong, W. Zhu, D.N. Sheng, K. Yang, Possible nematic spin liquid in spin-1 antiferromagnetic system on the square lattice: Implications for the nematic paramagnetic state of fese, Phys. Rev. B 95 (2017) 205132, https://doi.org/10.1103/PhysRevB.95.205132.
[49] S.R. White, Density matrix formulation for quantum renormalization groups, Phys. Rev. Lett. 69 (1992) 2863–2866, https://doi.org/10.1103/PhysRevLett. 69.2863.
[50] S.R. White, Density-matrix algorithms for quantum renormalization groups, Phys. Rev. B 48 (1993) 10345–10356.
[51] D. Dey, D. Maiti, M. Kumar, An efficient density matrix renormalization group algorithm for chains with periodic boundary condition, Papers Phys. 8 (2016).
[52] M. Kumar, Z.G. Soos, D. Sen, S. Ramasesha, Modified density matrix renormalization group algorithm for the zigzag spin-$\frac{1}{2}$ chain with frustrated antiferromagnetic exchange: Comparison with field theory at large J_2/J_1, Phys. Rev. B 81 (2010) 104406, https://doi.org/10.1103/PhysRevB.81.104406.
[53] M. Kumar, A. Parvej, S. Thomas, S. Ramasesha, Z.G. Soos, Efficient density matrix renormalization group algorithm to study y junctions with integer and half-integer spin, Phys. Rev. B 93 (2016) 075107 .
[54] M. Kumar, S. Ramasesha, Z.G. Soos, Density matrix renormalization group algorithm for bethe lattices of spin-$\frac{1}{2}$ or spin-1 sites with heisenberg antiferromagnetic exchange, Phys. Rev. B 85 (2012) 134415, https://doi.org/10.1103/PhysRevB.85.134415.
[55] R.T. Clay, A.W. Sandvik, D.K. Campbell, Possible exotic phases in the one-dimensional extended hubbard model, Phys. Rev. B 59 (1999) 4665–4679, https://doi.org/10.1103/PhysRevB.59.4665.
[56] S. Ejima, F. Gebhard, S. Nishimoto, Tomonaga-luttinger parameters for doped mott insulators, Europhys. Lett. 70 (4) (2005) 492 URL: http://stacks.iop.org/0295-5075/70/i=4/a=492.
[57] C. Cheng, B.-B. Mao, F.-Z. Chen, H.-G. Luo, Phase diagram of the one-dimensional t-j model with long-range dipolar interactions, Europhys. Lett. 110 (3) (2015) 37002.
[58] F. Pollmann, A.M. Turner, E. Berg, M. Oshikawa, Entanglement spectrum of a topological phase in one dimension, Phys. Rev. B 81 (2010) 064439, https://doi.org/10.1103/PhysRevB.81.064439.
[59] L. Guang-Hua, Z. Yu, T. Guang-Shan, Quantum phase transitions, entanglement spectrum, and schmidt gap in bond-alternative s = 1 antiferromagnetic chain, Commun. Theor. Phys. 61 (6) (2014) 759, https://doi.org/10.1088/0253-6102/61/6/16.
[60] A. Chandran, V. Khemani, S.L. Sondhi, How universal is the entanglement spectrum? Phys. Rev. Lett. 113 (2014) 060501, https://doi.org/10.1103/PhysRevLett.113.060501.